Photonic Polyethylene from Self-Assembled Mesophases of Polydisperse Olefin Block Copolymers

Phillip D. Hustad,* Gary R. Marchand, Eddy I. Garcia-Meitin, Patricia L. Roberts, and Jeffrey D. Weinhold*

The Dow Chemical Company, 2301 North Brazosport Boulevard, Freeport, Texas 77541

Received February 6, 2009; Revised Manuscript Received March 18, 2009

ABSTRACT: We have discovered a synthetic process capable of producing olefin block copolymers (OBCs) with controlled block length polydispersity. Certain compositions of these OBCs self-assemble in the melt to form ordered mesophases. The morphologies and dielectric contrast of the semicrystalline and amorphous blocks produce transparent films exhibiting a partial photonic band gap for frequencies in the visible spectrum. The domain spacings are not only much larger than expected for monodisperse block copolymers of similar molecular weight, but they also exceed the predictions of recent theories for polydisperse block copolymers. An extension to Strong Segregation Theory demonstrates that many molecules have a weak preference for segregation to the interface versus the center of a domain. Minor perturbations can then produce highly swollen but relatively stable domains.

Introduction

Many of the attractive features of block copolymers (BCPs) are derived from the ability to create hybrid macromolecules composed of blocks that are normally immiscible with each other. These macromolecules often self-assemble to form many complex nanoscale morphologies that impart interesting properties and enable a wide range of applications.[1,2] BCPs are most commonly synthesized using living polymerizations, which give polymers with very narrow polydispersity indices (PDI). While narrow polydispersity is normally desired in BCP synthetic protocols, a few recent reports have found that broader polydispersity can have a profound impact on phase behavior.[3−18] Specifically, broader polydispersity has been shown experimentally to increase domain size.[6−11]

Despite the indications that block length polydispersity may provide a novel tool for manipulation of BCP morphology, this area remains largely unexplored due to the comparative lack of techniques for synthesis of polydisperse BCPs relative to monodisperse BCPs. We have recently discovered two methods for preparation of new types of olefin block copolymers (OBCs) with block length polydispersity.[19,20] These processes utilize mechanisms referred to as chain shuttling and coordinative chain transfer polymerization (CCTP) to form OBCs in continuous reactors. With these new synthetic tools, we were eager to explore OBC compositions expected to give ordered morphologies, with particular interest in examining the effects of polydispersity on phase behavior.

Results and Discussion

Block Copolymer Design and Synthesis. As a platform to explore these effects, we targeted diblock OBCs based on ethylene and 1-octene with "hard" blocks of semicrystalline linear low density polyethylene (LLDPE) and "soft" blocks of ultra low density polyethylene (ULDPE).[20] When both blocks have PDI = 2, Self-Consistent Field theory (SCFT)[4,5] predicts that the minimum χN of the order−disorder transition should be $\chi N = 4$, where χ is determined by the difference in the molar 1-octene content of the blocks, defined as Δ_{C8}, and N corresponds to the number-average statistical segments per diblock. Factors such as molecular weight-dependent fluctuation corrections,[21] composition deviations, and especially "breakout" crystallization from a weakly segregated system[22] require a larger χN to achieve ordered crystalline phases. For a typical molecular weight and 50/50 composition, we estimate that Δ_{C8} in excess of 20 mol % will produce the desired morphology.[23]

With anticipation of achieving self-assembly in the melt, we synthesized two diblock OBCs with $\Delta_{C8} \approx 35$ mol % and weight fractions of LLDPE, f_{LLDPE}, near 0.5. The materials were prepared according to the procedure described by Hustad et al.[20] as outlined in Figure 1 using a pyridylamide-based catalyst system in conjunction with diethylzinc (DEZ) in a series of two continuous stirred tank reactors (CSTRs). Monomer compositions are independently controlled in the two CSTRs to provide the desired LLDPE and ULDPE compositions, and production rates are controlled to achieve the desired f_{LLDPE}. Samples 1 and 2 were prepared with different values of M_n by adjusting the DEZ feed, and a physical blend of LLDPE and ULDPE copolymers with similar composition (sample 3) was prepared by removing the DEZ. A material with lower Δ_{C8} (6.9 mol %, sample 4), which should not form a self-assembled melt, was also included for comparison.[20] This continuous process generated OBCs at a production rate of ca. 4 kg/h, yielding relatively large quantities of OBCs in short periods of time. Relevant characterization data of the OBCs are provided in Table 1, and further details of the synthesis can be found in the Supporting Information.

Self Assembly and Morphology. With materials in hand, we prepared compression molded films to examine the bulk morphologies with transmission electron microscopy (TEM). To prepare the films, pellets were preheated at 190 °C for 10 min, compressed at 20 000 lbf for 20 min, and then quenched at 15 °C without further annealing. Surprisingly, we immediately noticed an unusual coloration in the molded samples of the high Δ_{C8} OBC diblocks. The compression molded films shown in Figure 2 are imaged on either black or white backgrounds or through clear glass to demonstrate these effects. The samples are all colorless on white backgrounds, but samples 1 and 2 appear blue when viewed under ambient light against a black background and yellow when viewed in transmission in front of a white light source. These effects are absent in the physical blend (sample 3) and low Δ_{C8} diblock (sample 4). The differences in appearance in reflected and transmitted light

* To whom correspondence should be addressed. E-mail: pdhustad@dow.com (P.D.H.); jweinhold@dow.com (J.D.W.).

10.1021/ma9002819 CCC: $40.75
Published on Web 04/21/2009

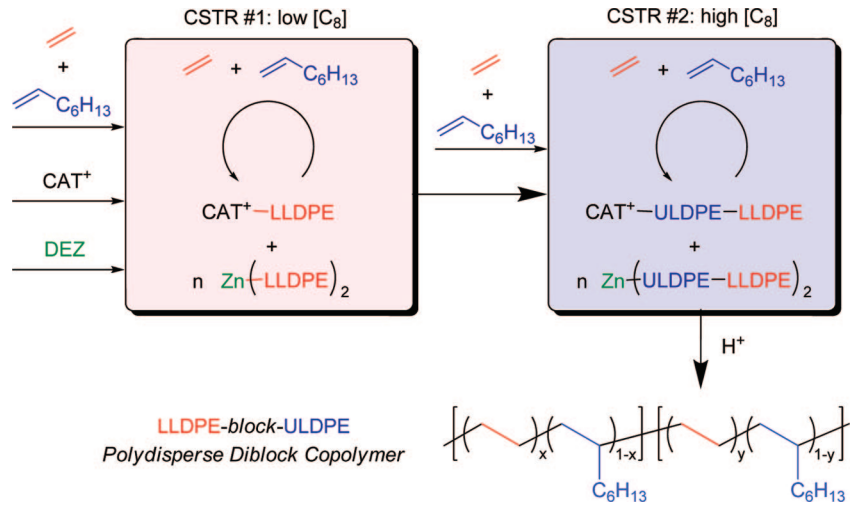

Figure 1. Reactor schematic for preparation of olefin-based diblock copolymers from CCTP in a series of CSTRs.

Table 1. Characterization Data for Ethylene-Based OBCs from the Dual-Reactor Process

sample	description	M_n (kg/mol)	PDI	f_{LLDPE} (wt %)	$C_{8(total)}$[a] (mol %)	Δ_{C8}[a]	$X_{c,\Delta H}$[b] (wt %)	D_{sp}[c] (TEM, nm)	D_{sp}[d] (reflect., nm)	λ_{PR} (obs., nm)	λ_{PR}[e] (TEM, nm)
1	high Δ_{C8} OBC	47.0	2.07	0.52	16.5	36	21	136 ± 12	124	369	406
2	high Δ_{C8} OBC	67.5	2.04	0.51	15.6	34	18	163 ± 24	143	428	486
3	blend	31.1	3.70	0.66	12.2	40	20	>10 000	n.d.[f]	n.o.[f]	n.o.[f]
4	low Δ_{C8} OBC	44.5	1.67	0.31	6.9	10	36	n.d.[f]	n.d.[f]	n.o.[f]	n.o.[f]
sample2/oil/LLDPEblend		n.a.[f]	n.a.[f]	n.a.[f]	n.a.[f]	n.a.[f]	n.d.[f]	205 ± 21	169	503	612

[a] Determined by ^{13}C NMR. [b] Crystallinity from the second heat of melting. [c] Average domain spacing as estimated from TEM micrographs. [d] Average domain spacing as estimated from the measured reflectance peak using eq 1. [e] Peak reflectivity, λ_{PR}, estimated using the average D_{sp} from TEM and eq 1. [f] n.a. = not applicable, n.d. = not detected, n.o. = not observed.

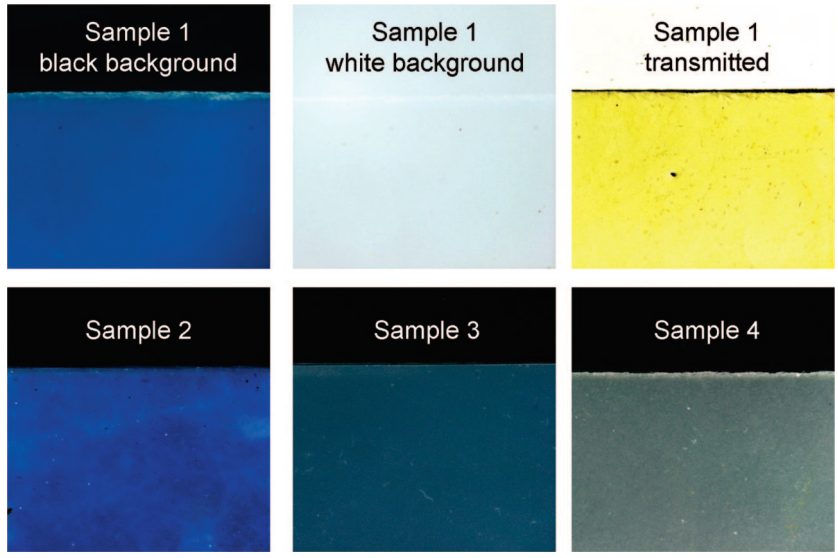

Figure 2. Optical images of compression molded films of samples 1−4.

suggested that the colors were not the result of an absorbing moiety but rather a scattering phenomenon.

Following these observations, the compression molded samples were subsequently stained with ruthenium tetraoxide (RuO_4) and sectioned for TEM analysis; representative images are shown in Figure 3. The physical blend, sample 3, exhibits a macrophase separated morphology typical of an immiscible blend of LLDPE and ULDPE. The semicrystalline LLDPE domain appears lighter in color due to the preferential staining of the ULDPE domains by the RuO_4. The low Δ_{C8} OBC diblock, sample 4, exhibits uniformly dispersed lamellar crystals similar to that of multiblock OBCs of similar crystallinity[24] and as expected when crystallization proceeds from a homogeneous melt. The high Δ_{C8} OBC diblocks, samples 1 and 2, exhibit morphologies consistent with self-assembled block copolymers, with ordered semicrystalline domains consistent with confined crystallization from the self-assembled melts. Sample 1 displays a well-ordered mesophase separated morphology resembling that of a lamellar structure with alternating LLDPE and ULDPE domains. Although defects are present, the domains are highly aligned across very large areas. Sample 2 also exhibits a mesophase separated morphology with a higher degree of discontinuity and more defects relative to sample 1. These TEM images clearly demonstrate the ability to design and synthesize polyethylene-based diblock materials, which form ordered morphologies from self-assembly.

After observing the ordered morphologies, our attention immediately turned to the unusually large sizes of the domains.

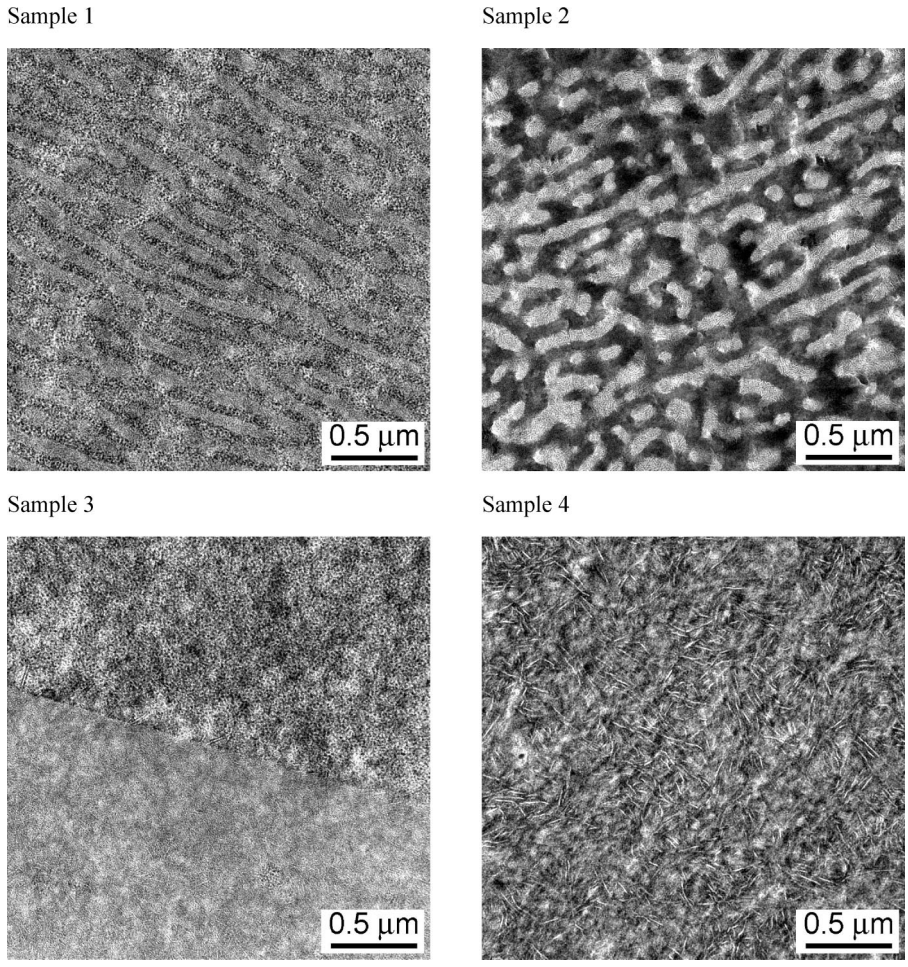

Figure 3. TEM images of sections taken from compression molded films of samples 1−4.

As shown in Figure 3, the high Δ_{C8} OBC diblocks, samples 1 and 2, exhibit average domain spacings (D_{sp}) of approximately 140 and 160 nm, respectively. Spacings of this magnitude are typical of materials with M_n's that are an order of magnitude higher; in fact, BCPs with similar M_n's typically have spacings in the 30−50 nm range. The domain spacings and levels of order in these simple unannealed compression molded films are remarkable considering the relatively low M_n's of the OBCs. The large spacings also supported our suspicions on the origins of the color in the films; these OBCs act as photonic crystals.

Photonic Properties. Photonic crystals are periodic dielectric materials that manipulate and control the movement of light.[25−27] A common photonic material is a multilayer stack composed of alternating layers of materials with contrast in refractive index, n. For a two-component A−B multilayer stack, the first-order wavelength of peak reflectivity at normal incidence, λ_{PR}, is a function of the optical thickness of each layer according to the following equation:

$$\lambda_{PR} = 2(n_A d_A + n_B d_B) \quad (1)$$

where n_A and n_B are the refractive indices of the two components, and d_A and d_B are the respective thicknesses. The refractive index of polyethylene varies with crystallinity, which is easily controlled by comonomer content. In these mesophase separated OBCs, the compositions of the LLDPE and ULDPE blocks correspond to values of n of 1.510 and 1.473, respectively. Utilizing these values of n and the estimated domain sizes from TEM, the predicted first-order wavelength of peak reflectivities according to eq 1 are 406 and 486 nm for samples 1 and 2, respectively.

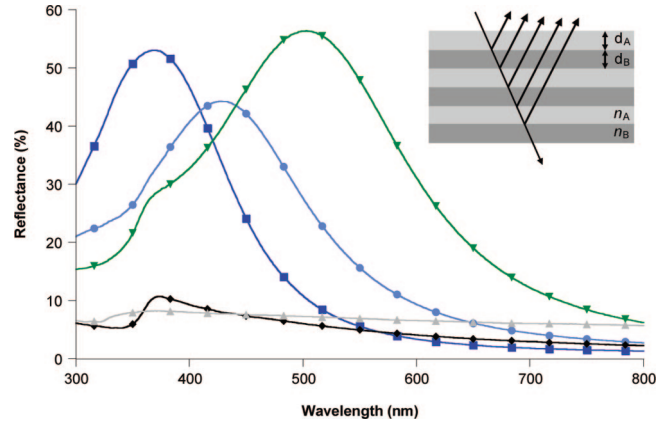

Figure 4. Reflectance spectroscopy of films of sample 1 (■), sample 2 (●), sample 3 (◆), sample 4 (▲), and a sample 2 blend containing 20 wt % oil and 20 wt % LLDPE (▼). The inset represents a schematic of the reflectance from a 1-D Bragg stack.

The reflectivities in the ultraviolet and visible (UV−vis) regions of the compression molded films were measured using a spectrophotometer equipped with an integrating sphere detector. As indicated in Figure 4, the physical blend and the low Δ_{C8} diblock both show less than ca. 10% reflectivity across the entire visible region, consistent with their lack of color. In contrast, the two high Δ_{C8} OBC diblocks exhibit well-defined peaks with reflectivities between 44% and 56% and peak positions at 369 and 428 nm for samples 1 and 2, respectively.[28] These values are in reasonable agreement with the calculated peak reflectivities based on the estimated domain sizes from

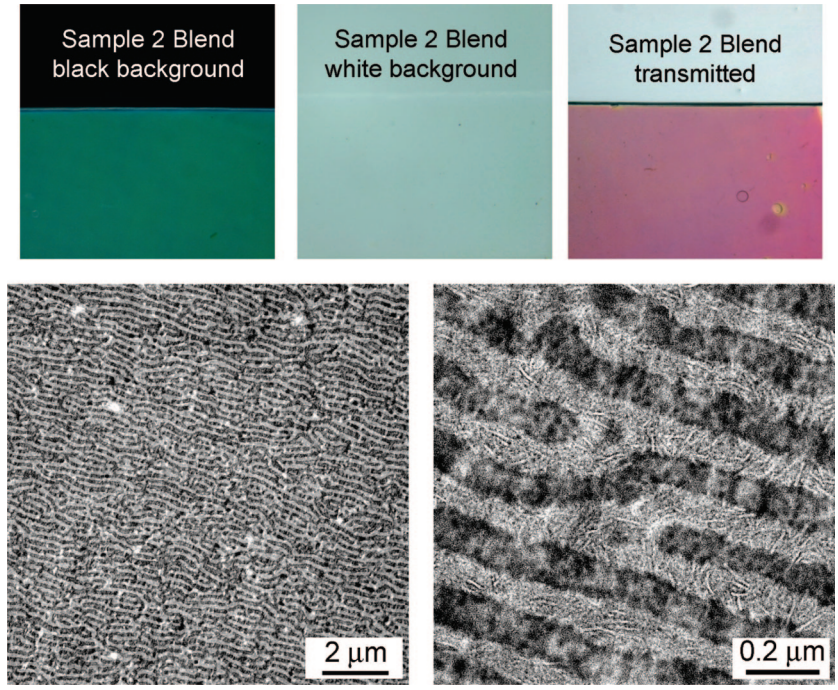

Figure 5. Photographs and TEM images of a blend of sample 2 with 20 wt % paraffinic oil and 20 wt % LLDPE. One interesting dislocation dipole is illustrated in the image with the 0.2 μm scale bar.

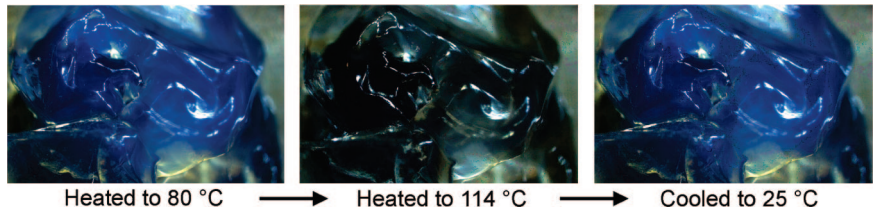

Figure 6. Optical images of a bulk piece of sample 1 at different temperatures, demonstrating the thermochromic response.

TEM, as are the domain spacings estimated from the observed λ_{PR}'s (Table 1). The observed blue shift in peak position may be attributed to a slight inaccuracy of measurement of domain spacing by TEM and/or misorientation of the mesophase separated structure from a perfect in-plane multilayer stack.

Although periodic structures of block copolymers have been used to fabricate photonic materials,[29−31] it has been a tremendous challenge to form ordered BCP morphologies with domain spacings large enough to interact with visible light.[29] The large periodicities required have only been achieved with conventional monodisperse BCPs of very high molecular weight.These materials typically have M_n's in excess of 500 000 g/mol and consequently require solution processing accompanied by long annealing times to achieve ordered morphologies that display well-defined visible reflectance peaks.[29,30] Our high Δ_{C8}, polydisperse OBCs exhibit morphological characteristics and photonic behavior similar to these high molecular weight, monodisperse BCPs at M_n's that are an order of magnitude lower.

In addition to facilitating large-scale solvent-free processing, lower molecular weights enable tailoring of the position of the reflectance peak[31] through introduction of swelling agents by melt blending.[32] As shown in Figure 4, the wavelength of peak reflectance shifts from 428 to 503 nm (from blue to green) by melt blending sample 2 with a low molecular weight LLDPE random copolymer (20 wt %, density = 0.91 g/cc) and a paraffinic oil (20 wt %). The images in Figure 5 demonstrate the coloration of the film, which appears green, pink, or colorless depending on the imaging technique. In addition, the compression molded film also exhibits an iridescence, indicating the presence of a more highly ordered lamellar structure compared to sample 2. This higher order is confirmed by the TEM images shown in Figure 5. In addition to the marked increase in spacing, with D_{sp} = 205 nm, the blend exhibits a substantial increase in long-range order with fewer defects and a higher degree of both positional and directional alignment as compared to sample 1. We tentatively attribute this increase in order to enhanced chain mobility generated by addition of the low molecular weight swelling agents.

In addition to the practical advantages of melt processing, another distinguishing feature of these photonic polyethylene-based OBCs arises from the semicrystalline nature of the LLDPE block. Crystallinity has been expressly avoided in other reported BCP photonic materials to limit undesired scattering, which could render the material opaque.[33] Despite their crystallinity, these high Δ_{C8} OBC films are highly transparent, transmitting more than 90% of light at permitted wavelengths.[34]

The crystallinity also imparts a distinctive thermochromic mechanism for the photonic characteristics.[35,36] In the melt, LLDPE and ULDPE are amorphous and therefore have the same n. Consequently, these materials lose their optical contrast as the samples are heated above their melting temperatures ($T_m \approx$ 100 °C). Figure 6 demonstrates this feature with a bulk piece of a pellet of sample 1. The reflected blue color is present at 80 °C but disappears upon melting of the LLDPE crystals. The color quickly returns as the material is cooled below the crystallization temperature, indicating that the aligned domain structure is preserved throughout the process. This behavior

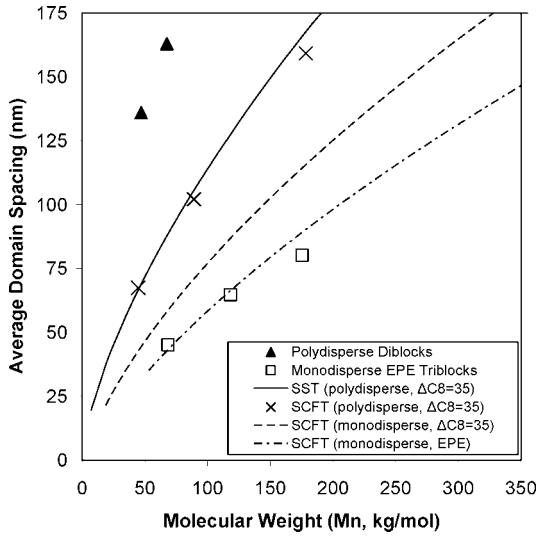

Figure 7. Domain size as a function of M_n for EO-based OBCs (▲), comparative monodisperse EPE triblocks[37] (□), predictions for EO (- - -) and EPE (- • -) compositions at 80 °C using monodisperse SCFT, and predictions from polydisperse SCFT (×) and SST (−) for EO compositions.

coupled with the high transparency of the films demonstrates a unique advantage to incorporation of a semicrystalline block into photonic BCP materials.

Phase Behavior in Polydisperse BCPs. While the TEM and reflectance measurements confirm the unexpectedly large domain sizes, they do not explain why they are so large. Some increase in domain size was expected due to block polydispersity,[6−11] but the magnitude is much larger than predicted. Thus, theories pertaining to the effects of polydispersity, composition, and molecular weight on domain sizes have been reexamined. Contributions from each of these factors are represented within Figure 7, which compares observed versus predicted domain spacings, D_{sp}, against M_n. To highlight the dramatic shift in this relationship, a comparative set of microphase separated BCPs with ethylene crystallinity and $f_{LLDPE} \approx 0.5$ are included.[37] These hydrogenated butadiene−isoprene−butadiene triblocks (EPE) are nearly monodisperse, and the molecular weights have been adjusted to approximate diblock behavior. At similar M_n, the EPE domain spacings are 2.5−3.6 times smaller than the polydisperse OBCs.

We began the exploration of these effects using self-consistent field theory (SCFT) for monodisperse BCPs.[38] The lowest line in Figure 7 corresponds to EPE triblocks using a characteristic ratio $C_\infty = 7.56$, as estimated from the individual blocks,[39] and χ from Koo et al.[37] As shown in the figure, this prediction is in good agreement with experiment for the EPEs. The dashed line at intermediate D_{sp} is the prediction for the monodisperse equivalent of samples 1 and 2. The calculation uses $C_\infty = 8.0$, corresponding to linear polyethylene at 80 °C, and χ based on extrapolation of neutron scattering results.[40] This trend is higher than that for EPE triblocks primarily because χ is larger. However, the observed spacings from samples 1−2 are still much higher than this prediction, indicating that the effect of composition on χ is not the primary source of the large domains.

To explore polydispersity effects on D_{sp}, a prediction based on Matsen's[11] adaptation of strong segregation theory (SST) to PDI = 2 in both blocks is shown as the solid line in Figure 7. The symbols in proximity to the SST line correspond to SCFT predictions[11] for $\chi N = 25$, 50, and 100. Both theories predict a substantial increase in domain spacing due to polydispersity. In SST, the increase is due to a reduction in the entropic penalty of stretching, F_{st}, of the blocks away from the interface. This

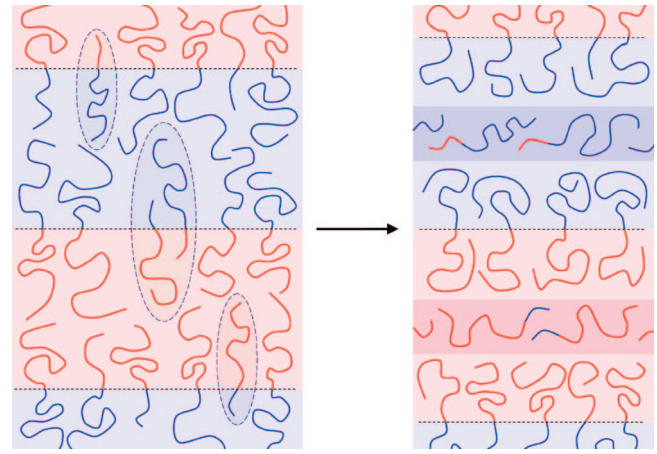

Figure 8. Cartoon showing the movement of molecules with large mismatch in block length away from the interface and into swelling layers.

effect changes the balance between minimal interfacial area and low F_{st} such that smaller interfacial areas with chains extending farther from the interface are now favored.

SCFT accounts for this effect as well as the swelling mechanism depicted in Figure 8.[10,11] Because individual diblocks have no correlation between block lengths, many molecules will have one block shorter, and the other block longer, than the respective average lengths. If these molecules are at the interface, the entropy lost by the longer block opposes the enthalpy gained by surrounding the short block with like segments. With large enough mismatch in length, the chemical potential drives these molecules away from the interface and swells the domains preferred by the longer blocks. This mechanism is expected to cause SCFT to predict higher D_{sp} than SST, but Figure 7 shows the predictions to be comparable. This is likely due to inaccuracy in the assumptions of SST, especially at $\chi N < 100$. Nevertheless, the key observation is that both theories predict substantially smaller domain spacings than the measured values for samples 1−2. Inaccuracy in input parameters, such as the effect of ULDPE blocks on C_∞, may account for a small portion of the disparity, but the magnitude of the difference strongly suggests that a new concept is necessary to explain the large domain spacings.

Although the spacing that produces the lowest free energy state has been the focus of most comparisons to theory, less attention has been devoted to the driving force for an ordered morphology to achieve that exact equilibrium spacing. Strong segregation theory provides a convenient way to evaluate the free energy both at and away from equilibrium. The theory assumes each molecule's block junction is located within a narrow region at the interface, which allows a lamellar mesophase to be treated as a system of planar interfaces with polymer brushes extending outward from both sides. Assuming that the overall composition is 50/50 and accounting for polydispersity,[11,41] the free energy, F, can be reduced to

$$\frac{\beta F}{n_T} = \left(\frac{\pi^2}{3}(\chi N_T)S\right)^{1/3}\left(\frac{1}{2}\left[\frac{D_{bo}}{D_b}\right] + \frac{1}{4}\left[\frac{D_b}{D_{bo}}\right]^2\right) \quad (2)$$

where $\beta = 1/kT$, n_T is the total number of molecules, N_T is the number-average backbone CH_2's per molecule, and S is a function of the probability, $p(\sigma)$, of having a block of length σ and is determined by[41]

$$S = \int_0^\infty d\sigma[1 - \int_0^\sigma d\sigma' \, p(\sigma')]^3 \quad (3)$$

D_b and D_{bo} are the actual and equilibrium brush heights, respectively, with D_{bo} given by[11]

$$D_{bo} = \frac{1}{2}\left(\frac{8\chi N_T}{3\pi^4 S^2}\right)^{1/6} aN_T^{0.5} \quad (4)$$

where $a = l\sqrt{C_\infty}$ is the statistical segment length, and $l = 0.154$ nm is the length of a bond. Using the convention that the number-average block length corresponds to $\sigma = 1$, eq 3 gives $S = 1$ for monodisperse blocks, and S decreases continually as the distribution is broadened; for a most probable distribution, $S = 1/3$.

The dependence of free energy versus domain spacing, $D_{sp} = 4D_b$, is shown in Figure 9 for monodisperse and polydisperse diblocks at $\chi N = 50$. At domain spacings smaller than the equilibrium value, both cases have nearly identical free energies because they are dominated by the product of interfacial tension ($\gamma_I \propto \sqrt{\chi N}$) and area. As area decreases further, the stretching penalty grows, but this contribution to free energy is proportional to S, causing F to increase more gradually in the polydisperse case. As a result, the free energy minimum moves to larger D_{sp}, and the well surrounding this equilibrium point becomes broader. The well's shape suggests that a polydisperse diblock at $D_b > D_{bo}$ could experience a slightly weaker drive to equilibrium than a monodisperse diblock. Although this reduced driving force may have a small effect, the measured D_{sp} values are approximately 90% higher than the predictions. Figure 9 indicates that a sample at 1.9 D_{bo} should experience a strong drive toward smaller spacing, but we have only observed a slight reduction in D_{sp} upon annealing.

Although strong segregation theory allows nonequilibrium spacings to be evaluated, the implementation in eq 2 neglects a key effect: the ability of molecules to leave the interface and swell domains. This mechanism may seem inconsistent with the principles of strong segregation; however, diblocks with PDI = 2 in both blocks and average $f_{LLDPE} = 0.5$ have a surprisingly broad composition distribution with, for example, just as many molecules at f_{LLDPE} of 0.05 as 0.5.[3a] After molecules from the fringes of this distribution move away from the interface, the remaining molecules are strongly segregated. To understand how this partitioning of molecules can affect morphology, an extension of strong segregation theory is proposed. As depicted in Figure 8, the system can be treated as three phases that consist of a layer of molecules segregated to the LLDPE/ULDPE interface and two disordered layers that are rich in either segment type and are located between brushes of the same composition. Mixing of segments at the boundaries between the brushes and the swelling layers is neglected because the key conclusions are unaffected by this property. Likewise, micelle formation within the swelling layers is ignored. To achieve nonequilibrium domain spacings, two forces are imposed on the interface: the normal interfacial tension and a lateral surface pressure, π_a. For a 50/50 diblock, the brush height is derived to be

$$D_b = \left(\frac{1}{2\pi^2}\left[\frac{\pi_a N_{in}^{0.5}}{a\rho} + \sqrt{\frac{\chi N_{in}}{6}}\right]\right)^{1/3} \frac{aN_{in}^{0.5}}{S^{1/3}} \quad (5)$$

where N_{in} is the average number of segments per molecule segregated to the interface, and ρ is the density of segments. The central objective of the model is to calculate the chemical potential, μ, of a molecule within each layer. The probability $\exp(-\beta\mu)$ then determines the partitioning of the molecule. The chemical potential within the interfacial layer is the most complex element. For a monodisperse diblock, removing any molecule from the interface simply changes the interfacial area without affecting other properties. In a polydisperse brush, each molecule is affected by all others through the variables N_{in}, S, and D_b. For example, the contribution to the chemical potential due to stretching is

$$\frac{\partial \beta F_{st,\alpha}}{\partial n_j} = \frac{\pi^2}{4}\left(\frac{1}{2\pi^2}\left[\frac{\pi_a N_{in}^{0.5}}{a\rho} + \sqrt{\frac{\chi N_{in}}{6}}\right]\right)^{2/3} S^{1/3}\left[1 + \frac{n_{in}}{3S}\frac{\partial S_\alpha}{\partial n_j} + \frac{1}{3}\left(\frac{N_j}{N_{in}} - 1\right)\right] \quad (6)$$

where n_{in} is the number of molecules at the interface, and the derivative of S is given by

$$\frac{\partial S}{\partial n_j} = \frac{1}{n_{in}}\left[3\int_0^{\sigma_j} d\sigma\, p(\sigma)[1 - p(\sigma)]^2 - 3\int_{\sigma_j}^{\infty} d\sigma[1 - p(\sigma)]^3\right] \quad (7)$$

A full derivation and discussion of the theory will be given in a separate publication.

This model, referred to as Extended SST, is solved through an iterative procedure. The system is initially configured with all molecules at the interface. A Monte Carlo routine generates the molecules and selects the blocks from a most probable distribution. The chemical potentials and partitioning of each molecule are then determined. After 200 000 molecules have been generated, variables such as S and N_{in} are calculated on the basis of the distribution of molecules remaining at the interface. The next iteration is then performed, and convergence is obtained quickly, usually in only 3−4 iterations.

Results from the theory at surface pressures $\pi_a \geq 0$ are included in Figure 9. To make direct comparisons to the trends from eq 2, the plotted free energies exclude the product of π_a and interfacial area.The Extended SST trend begins at the equilibrium solution, $\pi_a = 0$, which has a slightly lower free energy and a higher spacing ($D_{sp} = 4D_b n_T N_T / n_{in} N_{in}$) than standard SST's equilibrium point. Both effects could be expected on the basis of the new degree of freedom, which allows 10% of the volume to move out of the interfacial layer. The most important conclusions are drawn from the nonequilibrium states ($\pi_a > 0$). These configurations have large domain spacing, but, due to the ability of molecules to leave the interface, the free energy penalty is greatly reduced. This behavior derives from the fraction of molecules that, due to polydispersity, have nearly the same chemical potential at the interface as in one of the swelling layers. At equilibrium, most of these molecules are favored to remain at the interface; however, only a small perturbation is needed to drive these molecules to the swelling layers. The shear forces applied during pelletization and sample

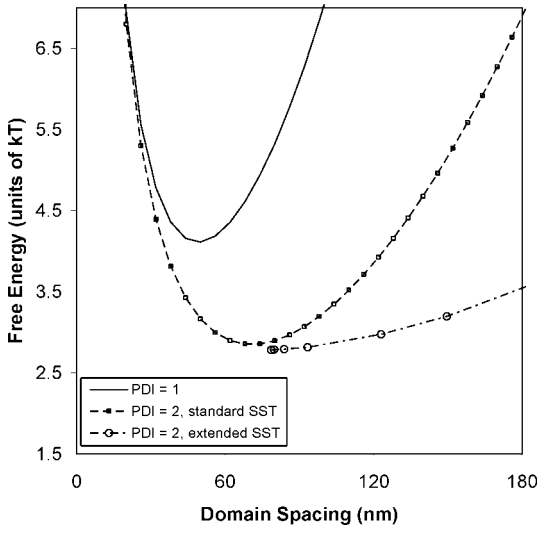

Figure 9. Free energy penalty of domain spacings that deviate from their equilibrium values at $\chi N = 50$, $f_{LLDPE} = 0.5$, and $M_n = 40$ kg/mol, including standard SST predictions for monodisperse (−) and polydisperse (- -□- -) diblocks, and polydisperse Extended SST results (- -○- -).

preparation can easily provide this perturbation. Based on the weak dependence of free energy on D_{sp} at $\chi N = 50$, domain spacings larger than the equilibrium value should be relatively stable. Higher values of χN will increase the slope between free energy and D_{sp}, thereby increasing the system's drive to find states closer to the equilibrium spacing. In continuing studies toward validating the proposed mechanism, we plan to evaluate this effect by preparing samples over a range of Δ_{C8} values.

Conclusion

The mesophase separated OBCs described here demonstrate some of the remarkable effects of polydispersity on the self-assembly of block copolymers. In fact, the unique domain spacing/molecular weight relationship exhibited by these materials reveals that these effects go beyond those previously imagined. Controlled polydispersity can be used to create materials with combinations of properties that are not possible with monodisperse BCPs, such as melt processable materials with very large domain spacings. The photonic polyethylene presented here represents an important step in the evolution of polyolefins toward high value applications. The capability to fabricate self-assembled structures with tailored domain spacings this large with solvent-free processes has significant implications on scalability and applicability of this technology. In addition, the need to extend block copolymer theory to explain the observations shows that there is still much to be learned from these polydisperse systems. The theory's results indicate that nonequilibrium effects may become more important as polydispersity is increased. This concept, combined with recent simulations[18] that emphasize the role of fluctuations on the order−disorder transition, suggest that accurate predictions of polydisperse BCP phase behavior will require more complex models than monodisperse systems. We are currently working to better understand the unique characteristics of these OBCs and imagine that further research will continue to uncover unexpected advantages of polydispersity in block copolymer systems.

Acknowledgment. We thank J. Bazen, T. Vink, Z. Zhou, S. Qiu, and A. Leugers for assistance with preparation and characterization of the OBCs, and B. Poon, R. Kuhlman, C. Li Pi Shan, K. Walton, B. Landes, L. Li, R. Register, S. Li, S. Foulger, and G. Fredrickson for helpful discussions.

Supporting Information Available: Additional experimental details for dual-reactor operation, polymer characterization details, additional TEM images, and transmittance spectra. This material is available free of charge via the Internet at http://pubs.acs.org.

References and Notes

(1) Bates, F. S. *Science* **1991**, *251*, 898–905.
(2) Bates, F. S.; Fredrickson, G. H. *Phys. Today* **1999**, *52*, 32–38.
(3) For an excellent review and highlight of recent work in this area, see: (a) Lynd, N. A.; Meuler, A. J.; Hillmyer, M. A. *Prog. Polym. Sci.* **2008**, *33*, 875–893. (b) Hillmyer, M. A. *J. Polym. Sci., Part B: Polym. Phys.* **2007**, *45*, 3249.
(4) Burger, C.; Ruland, W.; Semenov, A. N. *Macromolecules* **1990**, *23*, 3339–3346.
(5) Potemkin, I. I.; Panyukov, S. V. *Phys. Rev. E* **1998**, *57*, 6902.
(6) Bendejacq, D.; Ponsinet, V.; Joanicot, M.; Loo, Y. L.; Register, R. A. *Macromolecules* **2002**, *35*, 6645–6649.
(7) Sides, S. W.; Fredrickson, G. H. *J. Chem. Phys.* **2004**, *121*, 4974.
(8) Lynd, N. A.; Hillmyer, M. A. *Macromolecules* **2005**, *38*, 8803–8810.
(9) Noro, A.; Cho, D.; Takano, A.; Matsushita, Y. *Macromolecules* **2005**, *38*, 4371–4376.
(10) Cooke, D. M.; Shi, A. C. *Macromolecules* **2006**, *39*, 6661–6671.
(11) Matsen, M. W. *Eur. Phys. J. E* **2006**, *21*, 199.
(12) Matsen, M. W. *Phys. Rev. Lett.* **2007**, *99*, 148304.
(13) Lynd, N. A.; Hillmyer, M. A. *Macromolecules* **2007**, *40*, 8050–8055.
(14) Meuler, A. J.; Ellison, C. J.; Evans, C. M.; Hillmyer, M. A.; Bates, F. S. *Macromolecules* **2007**, *40*, 7072–7074.
(15) Lynd, N. A.; Hamilton, B. D.; Hillmyer, M. A. *J. Polym. Sci., Part B: Polym. Phys.* **2007**, *45*, 3386–3393.
(16) Meuler, A. J.; Ellison, C. J.; Hillmyer, M. A.; Bates, F. S. *Macromolecules* **2008**, *41*, 6272–6275.
(17) Lynd, N. A.; Hillmyer, M. A.; Matsen, M. W. *Macromolecules* **2008**, *41*, 4531–4533.
(18) Beardsley, T.; Matsen, M. *Eur. Phys. J. E* **2008**, *27*, 323–333.
(19) Arriola, D. J.; Carnahan, E. M.; Hustad, P. D.; Kuhlman, R. L.; Wenzel, T. T. *Science* **2006**, *312*, 714–719.
(20) Hustad, P. D.; Kuhlman, R. L.; Arriola, D. J.; Carnahan, E. M.; Wenzel, T. T. *Macromolecules* **2007**, *40*, 7061–7064.
(21) Fredrickson, G. H.; Helfand, E. *J. Chem. Phys.* **1987**, *87*, 697–705.
(22) Loo, Y. L.; Register, R. A. In *Developments in Block Copolymer Science and Technology*; Hamley, I. W., Ed.; John Wiley & Sons, Ltd.: New York, 2004.
(23) The minimum value was determined using solubility parameters derived from small-angle neutron scattering as a linear trend in the 1-octene mol % while setting $\chi N = 8$, temperature = 100 °C, 50/50 composition, and a backbone M_n of 55 kg/mol.
(24) Wang, H. P.; Khariwala, D. U.; Cheung, W.; Chum, S. P.; Hiltner, A.; Baer, E. *Macromolecules* **2007**, *40*, 2852.
(25) Yablonovitch, E. *Phys. Rev. Lett.* **1987**, *58*, 2059–2062.
(26) John, S. *Phys. Rev. Lett.* **1987**, *58*, 2486–2489.
(27) Joannopoulos, J. D.; Johnson, S. G.; Winn, J. N.; Meade, R. D. *Photonic Crystals: Molding the Flow of Light*, 2nd ed.; Princeton University Press: Princeton, 2008.
(28) It is important to note that below approximately 370 nm, the absorption of UV light by the residual zinc oxide and phenolic antioxidants interferes with both the % reflectivity and the transmittance of the films.
(29) Edrington, A. C.; Urbas, A. M.; DeRege, P.; Chen, C. X.; Swager, T. M.; Hadjichristidis, N.; Xenidou, M.; Fetters, L. J.; Joannopoulos, J. D.; Fink, Y.; Thomas, E. L. *Adv. Mater.* **2001**, *13*, 421–425.
(30) Fink, Y.; Urbas, A. M.; Bawendi, M. G.; Joannopoulos, J. D.; Thomas, E. L. *J. Lightwave Technol.* **1999**, *17*, 1963–1969.
(31) Urbas, A.; Fink, Y.; Thomas, E. L. *Macromolecules* **1999**, *32*, 4748–4750.
(32) Winey, K. I.; Thomas, E. L.; Fetters, L. J. *Macromolecules* **1991**, *24*, 6182–6188.
(33) Yoon, J.; Mathers, R. T.; Coates, G. W.; Thomas, E. L. *Macromolecules* **2006**, *39*, 1913–1919.
(34) Further details can be found in the Supporting Information.
(35) Osuji, C.; Chao, C. Y.; Bita, I.; Ober, C. K.; Thomas, E. L. *Adv. Funct. Mater.* **2002**, *12*, 753–758.
(36) Kang, Y.; Walish, J. J.; Gorishnyy, T.; Thomas, E. L. *Nat. Mater.* **2007**, *6*, 957–960.
(37) Koo, C. M.; Wu, L.; Lim, L. S.; Mahanthappa, M. K.; Hillmyer, M. A.; Bates, F. S. *Macromolecules* **2005**, *38*, 6090–6098.
(38) Matsen, M. W.; Bates, F. S. *Macromolecules* **1996**, *29*, 1091.
(39) Fetters, L. J.; Lohse, D. J.; Garcia-Franco, C. A.; Brant, P.; Richter, D. *Macromolecules* **2002**, *35*, 10096–10101.
(40) Reichart, G. C.; Graessley, W. W.; Register, R. A.; Lohse, D. J. *Macromolecules* **1998**, *31*, 7886.
(41) Milner, S. T.; Witten, T. A.; Cates, M. E. *Macromolecules* **1989**, *22*, 853.

MA9002819